Journal of Materials Chemistry C

An overview of oxygen vacancy dynamics in (1-x)(Bi1/2Na1/2)TiO3-xBaTiO3 solid solution

Journal:	*Journal of Materials Chemistry C*
Manuscript ID	TC-ART-06-2021-002668.R1
Article Type:	Paper
Date Submitted by the Author:	12-Jul-2021
Complete List of Authors:	Fan, Zhongming; Penn State University Park Randall, Clive; Penn State University Park

An overview of oxygen vacancy dynamics in (1-x)$(Bi_{1/2}Na_{1/2})TiO_3$-x$BaTiO_3$ solid solution

Zhongming Fan* and Clive A Randall

Materials Research Institute, Pennsylvania State University, University Park, Pennsylvania 16802, USA

*zbf5066@psu.edu

Abstract

The $(Bi_{1/2}Na_{1/2})TiO_3$ (BNT) based ceramics have been the hot topic for a few years because of their multiple functions, from the piezoelectric properties to more recently the electrostatic energy storage performance. However, some basic issues are still unclear, preventing the wide application in real devices. One of them is the underlying conduction mechanism, the interplay of electronic and ionic carriers as a mixed ionic case and the subsequent quantification. This paper deals with the most basic compositions, which are the typical ones from the (1-x)$(Bi_{1/2}Na_{1/2})TiO_3$-x$BaTiO_3$ (BNT-xBT) phase diagram. The conductivity is primarily investigated by impedance spectroscopy while different equivalent circuits are applied to different conduction mechanisms. A transition from predominantly ionic to predominantly electronic conduction is revealed to occur with the increase of $BaTiO_3$ concentration. The mixed ionic-electronic conduction in the composition near morphotropic phase boundary, namely BNT-7%BT, is identified and then quantified. To verify our interpretation of impedance results, dc degradation is, for the first time, conducted to this family of materials, from which the electronic and ionic conductions are easily separated by accessing the mean time to failure. The successful combination of the two methods enables us to have an overview of how the oxygen vacancy dynamics in the BNT-xBT system depends upon the phase nature or the domain structure.

1. Introduction

Over the past twenty years there has been dramatic development of lead-free ferroelectric ceramics.[1] So far, the community has recognized several base compositions that deserve extensive investigations, e.g. $(K_{1/2}Na_{1/2})NbO_3$ (KNN), $(Bi_{1/2}Na_{1/2})TiO_3$ (BNT), $BaTiO_3$ (BT), $AgNbO_3$ (AN), etc. [2-5] Among them, BNT stands out for its multifunctionality: $d_{33} \sim 200$ pC/N is achieved at morphotropic phase boundary in various solid solutions;[6] large electro-strain is observed near the depolarization temperature;[7] high levels of ionic conductivity is endowed by the acceptor doping;[8] good energy storage density and efficiency is realized in the so called "relaxor antiferroelectric" phase.[9] Generally speaking, understanding the oxygen vacancy dynamics is of great importance for electroceramics. First, in the case of BNT the high volatility of Bi and Na naturally facilitates the formation of oxygen vacancies during high temperature sintering,[10] while the weak Bi-O binding gives rise to the structural instability hence provides high oxygen vacancy mobility.[11] Second, the aforementioned properties of BNT always require a prolonged exposure to an electric field, which makes the reliability issue a major concern as oxygen vacancies can electromigrated through the material.

In 2013, Sinclair's group first characterized the excellent ionic conduction in BNT and later on demonstrated the tunability of its conductivity via adding aliovalent dopants or adjusting Bi/Na stoichiometry.[10,12] They primarily employed the electromotive force (EMF) to measure the oxygen ionic transport number and accordingly classified different BNT into three types, (I) predominantly ionic conduction; (II) mixed ionic-electronic conduction; (III) predominantly electronic conduction.[13] Regular BNT belongs to type I. Adding subtle amount of Nb^{5+} donor or excess Bi, BNT evolves to type II. It eventually becomes type III with further addition.[12] Compared with pure BNT, BNT-based solid solutions are more widely used.[6] Unless being doped with acceptors, common binary/ternary solid solutions are always claimed to be type III, where the single semicircle in Impedance Spectroscopy (IS) is interpreted as electronic conduction.[14] However, the interconnection of type I to III transition is not appreciated with respect to the phase diagram of a solid solution.

The objective of this work is to further investigate the composition dependence of the conduction mechanism across the phase diagram. In this paper, we are employing a dedicated equivalent circuit that can readily separate the ionic and electronic contributions to the total conductivity in IS. A critical concern immediately arises: is our interpretation valid and sufficient, relative to the methods used earlier on the ionic conductivity of BNT namely EMF and tracer diffusion. Here we further employ a dc degradation to potentially serve as a solid evidence. DC degradation is a process in which the oxygen vacancies are migrating towards the cathodic blocking electrode under a constant electric bias, accompanied by the increase of leakage current.[15] Thus, the activation energy for oxygen vacancy migration can be known as it governs the degradation process. The standard method is Highly Accelerated Lifetime Test (HALT) where the constant bias is applied at different elevated temperatures.[16] The mean time to failure (MTTF), namely the moment when the leakage current takes off, is defined as when the leakage current increases by a factor of ten. Knowing this, the activation energy can be calculated by fitting MTTF data to the Eyring equation,

$$\frac{t_1}{t_2} = \left(\frac{V_2}{V_1}\right)^n \exp\left[\frac{E_a}{k}\left(\frac{1}{T_1} - \frac{1}{T_2}\right)\right], \quad (1)$$

where t_i is the MTTF under electric bias V_i at temperature T_i; E_a is the activation energy; k is Boltzmann constant; n is the voltage acceleration factor. For a given voltage, Eq. (1) reduces to the Arrhenius model,

$$\frac{t_1}{t_2} = \exp\left[\frac{E_a}{k}\left(\frac{1}{T_1} - \frac{1}{T_2}\right)\right]. \quad (2)$$

The solid solution we choose to study is the most classic one, $(1\text{-}x)(Bi_{1/2}Na_{1/2})TiO_3\text{-}xBaTiO_3$ (BNT-xBT). Fig. 1 displays a simplified phase diagram.[17] Pure BNT is *R3c* phase, despite that some researchers believe it to be *Cc*.[18] The morphotropic phase boundary resides in a range from x = 6% to 11%. The highest $d_{33} \sim 180$ pC/N is seen in BNT-7%BT, attributed to the coexistence of *R3c* and *P4bm* phases. Further to the right, BNT-15%BT has entered the *P4mm* phase region. The corresponding dielectric measurements are inserted in the phase diagram. Both pure BNT and BNT-7%BT feature obvious frequency dispersion at low temperature, whereas BNT-15%BT shows just a little. In this work, we examine the oxygen vacancy dynamics in these three typical compositions, systematically.

2. Experimental

The pure BNT, BNT-7%BT, BNT-15%BT and BNT-15%BT-1%Ga ceramics were fabricated using conventional solid state reaction method, with starting powders of Bi_2O_3 (>99.9%), Na_2CO_3 (>99.95%), TiO_2 (>99.9%), $BaCO_3$ (>99.8%) and Ga_2O_3 (>99.99%) weighted according to the stoichiometry. The mixed powders were ball milled in ethanol for 24 hours both before and after being calcined as 850 ^oC for 2 hours. The sintering was carried out at 1150-1200 ^oC for 2 hours with the green pellet unburied by any protective powder. The sintered ceramics were slowly cooled down with furnace to avoid any quenching effects that have been found able to increase the conductivity in BNT. The as sintered pellets were polished to ~ 1 mm in thickness before platinum electrodes were sputtered. The IS was performed in a computer-controlled furnace with a Solartron ModuLab XM impedance analyzer from 0.1 Hz to 1 MHz. The HALT was conducted by applying constant electric bias to the ceramics at elevated temperatures while the leakage current was read by Keithley 2700. The domain structure of the ceramics was checked using Transmission Electron Microscopy (TEM) on Talos F200X (FEI). The TEM specimens were prepared by ion milling (PIPS II, Gatan) followed by an annealing at 500 ^oC to remove any possible impacts from the thermal history.

3. Results and discussion

The impedance of pure BNT is relatively straightforward to analyze, but here we use it matching IS and HALT data, to understand the transient changes as degradation proceeds. Following Sinclair,[10] we use two resistor-constant phase elements (R-CPE), that respectively represents the grain and grain boundary, connected in series to perfectly fit the two semi-circles in IS (Fig. 2a,b). The Arrhenius plot of the grain conductivity is shown in Fig. 2c and the activation energy is ~ 0.87 eV, suggesting the ionic conduction. HALT is done to pure BNT at 100, 125 and 150 ^oC under 3kV/cm (Fig. 2d). Initially, the current rises slowly. Subsequently, the increase of the current becomes more rapid until it slows down again. Eventually, a plateau is reached. Such a re-stabilization of the conductivity is commonly observed in the acceptor doped perovskites during dc degradation, which is ascribed to the redox reactions that take place within the cathodic/anodic layer.[19] We have noted that the reduction are not just at the interface, and the depth has variations with different compositions. We will present detailed discussion regarding this in a separate paper. The short arrows in Fig. 2d mark the MTTFs at different temperatures, which are then fitted according to Eq. (2) in Fig. 2e. The activation energy is calculated to be ~ 0.85 eV, in good consistence with the value obtained from IS (Fig. 2c). Several things can be concluded here: first, pure BNT indeed features predominantly ionic conduction (type I) due to the high concentration/mobility of oxygen vacancies; second, the dc degradation in pure BNT is governed by the electromigration of oxygen vacancies, inferred by the activation energy; third, HALT turns out to be a convenient way to extract the ionic conductivity, if any, from the total conductivity, therefore providing a powerful tool for studying the mixed conduction (type II) in combination with IS.

Similar investigations are carried out in BNT-7%BT. The Z* plot in Fig. 2a shows only one semicircle, which has been interpreted as the bulk resistance. However, unlike pure BNT, the semicircle in BNT-7%BT is so distorted that a single R-CPE cannot generate a satisfactory fitting result. Note that if the Arrhenius fitting is done with the bulk resistance that is simply extracted from the intercept of Z' axis, we can still obtain an activation energy. However, the mixed conductivities can by no means be easily separated. In order to reveal the distortion in the semi-circle more clearly, impedance is replotted in the electric modulus formalism, $M^* = j\omega C_0 Z^*$. As can be seen in Fig. 3b, $M''(f)$ is asymmetric due to an obvious “shoulder” at high frequency. It should be noted that we are not the first group to discover such “shoulder” in BNT-based solid solutions. Previously, this shoulder was attributed to an additional dielectric relaxation of the polar nanoregions, indicated by the successful fitting to the Vogel-Fulcher rather than Arrhenius equation.[20] Here we propose an alternative interpretation, the “shoulder” originates from ionic conduction. Given that ionic species are blocked at the electrode while the electronic species are permeable at the electrode, the ionic and electronic conduction are then separatable.[21-24] The equivalent circuit we used here is composed of three rails: the first rail represents the electronic resistance R_e; the second rail is the bulk capacitance C_1, the third rail consists of the series connection of the ionic resistance and the interface capacitance R_i-CPE_1. At high frequency, the ionic rail is conductive hence the total resistance is $(R_e^{-1} + R_i^{-1})^{-1}$. At low frequency, the ionic species have time to accumulate at the electrode and the impedance approaches R_e in the dc limit. Fig. 3c displays the temperature dependence of the electronic and ionic conductivity, of which the activation energies are $E_{a\,(\mathrm{ion})} \sim 0.76$ eV and $E_{a\,(\mathrm{ele})} \sim 1.08$ eV, respectively. To verify our interpretation and results, HALT is done at 200, 225, 250 ^{o}C under 5 kV/cm (Fig. 1d). Similar to the pure BNT, the leakage current in BNT-7%BT increases with time, first slowly then rapidly. However, an important difference from pure BNT is the absence of a plateau (note that the horizontal tails are because of the current limit of the system). As explained above, the conductivity re-stabilization is often seen in acceptor doped perovskites that have sufficient ionic electromigration to induce dramatic redox reactions near the electrodes, which is not the case in BNT-7%BT as a mixed conductor. Nevertheless, in the BNT-7%BT doped with acceptor dopants, the ionic conduction becomes predominant while the impedance data is qualitatively identical to that of pure BNT.[14] In those compositions, a plateau appears in the final stage of degradation. This will be discussed in more details in a separate paper. The activation energy of ionic conduction is calculated, by fitting the MTTFs (marked by the small arrows), to be ~ 0.76 eV. In terms of the dc conductivity (electronic), the initial leakage currents (marked by the small circles) are accessed through,

$$J = J_0 \exp\left[\frac{-E_a}{kT}\right], \tag{3}$$

while the activation energy is ~ 1.08 eV (Fig. 3e). Both values are exactly same as the ones obtained from IS, indicating that our selection of equivalent circuit and the fitting results are valid. On the other hand, in the acceptor doped BNT-7%BT (type I), the activation energy for the ionic conduction, obtained via fitting with the two R-CPE equivalent circuit (Fig. 2), lies in the range of 0.75 – 0.79 eV, which also shows that our result (~ 0.76 eV) in undoped case is reasonable. While in the Ta^{5+} doped BNT-7%BT (type III), the “shoulder” disappears and $M''(f)$ is symmetric. This again supports our interpretation that the “shoulder” is originated from ionic conduction which will be greatly suppressed by donor doping.

Fig. 4 examines the case of BNT-15%BT. The undistorted semi-circle and the symmetric $M''(f)$ with the absence of any “shoulder” along with the activation energy ~ 1.40 eV suggest BNT-15%BT a type III predominantly electronic conductor with nearly intrinsic semiconducting behavior (Fig 4a-c). The lower activation energy for the electronic conduction in BNT-7%BT should be due to its relatively larger defects concentration. So far, a type I (ionic) to type II (mixed) to type III (electronic) transition has been completely identified in the BNT-xBT solid solution. However, if we still want to learn more about the oxygen vacancy dynamic in BNT-15%BT, we need to add acceptor dopants to make it type I. Fig. 4d is the dielectric constant measured in BNT-15%BT-1%Ga, from which we learn that the phase nature of BNT-15%BT-1%Ga is unchanged compared with the undoped BNT-15%BT (inset of Fig. 1). They both are ferroelectric at low temperature and relaxor at high temperature, even the phase transition temperatures are the same, ~ 210 ^{o}C. The impedance of BNT-15%BT-1%Ga appears analogous to that of pure BNT and is therefore analyzed using same method. The Arrhenius plot has two regimes with distinct activation energies, ~ 0.93 eV below 210 ^{o}C and ~ 0.72 eV above 210 ^{o}C (Fig. 4e). 0.93 eV is never seen in any composition above, but 0.72 eV is very close to the value in BNT-7%BT. Therefore, it suggests that the oxygen vacancy dynamics in BNT is dependent upon the phase nature.

To extend the discussion, let us first summarize the activation energies for oxygen vacancy migration that we have obtained so far. The smallest E_a (< 0.8 eV) are found in BNT-7%BT and BNT-15%BT above the ferroelectric to relaxor transition temperature; the intermediate E_a (between 0.8 and 0.9 eV) is found in pure BNT; the largest E_a (> 0.9 eV) is found in BNT-15%BT below the transition temperature. It can be seen from the phase diagram (Fig. 1) that pure BNT is *R3c* phase, BNT-7%BT is on the *R3c*/*P4bm* phase boundary, BNT-15%BT is also *P4bm* phase at high temperature while is *P4mm* at low temperature. Meyer et al. used DFT calculation to show that the oxygen vacancy migration barriers are different in rhombohedral, orthorhombic and tetragonal phases in BNT.[25] Our systematic investigation in the BNT-xBT solid solution leads to a similar conclusion, $E_{a\,(P4mm)} > E_{a\,(R3c)} > E_{a\,(P4bm)}$ (Fig. 5). Another possible cause is related to the changes in domain structure. The grains in BNT-15%BT are full of large twinned ferroelectric domains of lamellar shape (Fig. 5a). The domain morphology in pure BNT was always described as "complex domains" (Fig .5b).[26] In fact, the complexity is resulted from the coexistence of smaller ferroelectric domains and dense antiphase boundaries. BNT-7%BT features the polar nanoregions instead of normal ferroelectric domains (Fig. 5c), and such microstructure presumably dominates in BNT-15%BT after the ferroelectric domains vanish above the transition temperature. It is well known that the ferroelectric domain walls are often not completely neutralized, which gives rise to the electrostatic interaction with the positively charged oxygen vacancy.[27,28] Once an oxygen vacancy is trapped at a well-defined ferroelectric domain wall, it requires more energy to hop out, namely a higher activation energy, as modelled earlier by Cao et al.[29] In the relaxor phase, on the contrary, the ferroelectric domains are disrupted so that the "blocking" force from the domain wall might become weaker, which makes the ionic hopping easier so that the activation energy drops. However, whether the polar nanoregions or other microstructural entities in BNT-based relaxors exert additional barrier to the ionic hopping is currently under investigation.

5. Conclusions

The oxygen vacancy dynamics are systematically examined in the BNT-xBT solid solution. A transition from ionic conductor through mixed conductor to electronic conductor is determined as x increases from 0 (< MPB) through 7% (= MPB) to 15% (> MPB). The ionic and electronic conductivity in BNT-7%BT are separated using a dedicated equivalent circuit. More importantly, such interpretation is validated by the DC degradation study, which is demonstrated to be an easy way to extract the ionic contribution from the total conduction. Therefore, the comparison of oxygen vacancy dynamics in different phases/domain structures is made possible. The activation energy for oxygen vacancy migration is, from the largest to the smallest, *P4mm*/big ferroelectric domains, *R3c*/complex domains and *P4bm*/polar nanoregions.

Acknowledgements

This work is supported by the National Science Foundation, as part of the Center for Dielectrics and Piezoelectrics under Grant Nos. IIP-1841453 and 1841466.

---

1 J. Rödel, W. Jo, K. Seifert, E. Anton, T. Granzow and D. Damjanovic, *J. Am. Ceram. Soc.*, 2009, **92**, 1153-1177.

2 Y. Saito, H. Takao, T. Tani, T. Nonoyama, K. Takatori, T. Homma, T. Nagaya and M. Nakamura, *Nature*, 2004, **432**, 84-87

3 GO. Jones and PA. Thomas, *Acta Crystallogr. B*, 2002, **58**, 168-178.

4 W. Liu and X. Ren, *Phys. Rev. Lett.*, 2009, **103**, 257602.

5 HU. Khan, K. Alam, M. Mateenullah, T. Blaschke, BS. Haq, *J. Eur. Ceram. Soc.* 2015, **35**, 2775-2789.

6 Y. Hiruma, H. Nagata and T. Takenaka, *J. Appl. Phys.*, 2008, **104**, 124106.

7 W. Jo, T. Granzow, E. Aulbach, J. Rödel and D. Damjanovic, *J. Appl. Phys.*, 2009, **105**, 094102.

8 F. Yang, M. Li, L. Li, P. Wu, E. Pradal-Velázque and DC. Sinclair, J. Mater. Chem. A 2017, **5**, 21658-21662.

9 J. Li, F. Li, Z. Xu and S. Zhang, *Adv. Mater.*, 2018, **30**, 1802155.

10 M. Li, MJ. Pietrowski, RA. De Souza, H. Zhang, IM. Reaney, SN. Cook, JA. Kilner and DC. Sinclair, *Nat. Mater.*, 2014, **13**, 31-35.

11 D. Schütz, M. Deluca, W. Krauss, A. Fetira, T. Jackson and K. Reichmann, *Adv. Funct. Mater.*, 2002, **22**, 2285-2294.

12 L. Li, M. Li, H. Zhang, IM. Reaney and DC. Sinclair, *J. Mater. Chem. C*, 2016, **4**, 5779-5786.

13 L. Li, M. Li, IM. Reaney and DC. Sinclair, *J. Mater. Chem. C*, 2017, **5**, 6300-6310.

14 S. Steiner, I. Seo, P. Ren, M. Li, DJ. Keeble and T. Frömling, *J. Am. Ceram. Soc.*, 2019, **102**, 5295-5304.

15 R. Waser, T. Baiatu and K. Härdtl, *J. Am. Ceram. Soc.*, 1990, **73**, 1645-1653.

16 S. Zhao, SJ. Zhang, W. Liu, NJ. Donnelly, Z. Xu and CA. Randall, *J. Appl. Phys.*, 2009,*105*, 053705.

17 C. Ma, X. Tan, E. Dul'kin and M. Roth, *J. Appl. Phys.*, 2010, **108**, 104105.

18 C. Ma, H. Guo and X. Tan, *Adv. Funct. Mater.*, 2013, **23**. 5261-5266.

19 R. Waser, T. Baiatu and K. Härdtl, *J. Am. Ceram. Soc.*, 1990, **73**, 1654-1662.

---

20 J. Zang, M. Li, DC. Sinclair, T. Frömling, W. Jo and J. Rödel, *J. Am. Ceram. Soc.*, 2014, **97**, 2825-2831.

21 NJ. Donnelly and CA. Randall, *Appl. Phys. Lett.*, 2010, **96**, 052906.

22 J. Jamnik and J. Maier, Phys. *Chem. Chem. Phys.*, 2011, **3**, 1668-1678.

23 J. Jamnik and J. Maier, *J. Electrochem. Soc.*, 1999, **146**, 4183.

24 C. Slouka, G. Holzlechner, L. Andrejs, E. Navickas, H. Hutter, J. Fleig, *J. Am. Ceram. Soc.*, 2015, **98**, 3259-3269.

25 K. Meyer and K, Able, *J. Mater. Chem. A*, 2017, **5**, 4368-4375.

26 H. Qi, R. Zuo, X. Zhou, D. Zhang, *J. Alloys Compd.*, 2019, **802**, 6-12.

27 C. Paillard, G. Geneste, L. Bellaiche and B. Dkhil, *J. Phys. Condens. Matter*, 2017, **29**, 485707.

28 Z. Fan, S. Zhang and X. Tan. *J. Eur. Ceram. Soc.*, 2020, **40**, 1217-1222.

29 Y. Cao, J. Shen, CA. Randall, LQ. Chen, *Acta Mater.*, 2016, **112**, 224-230.

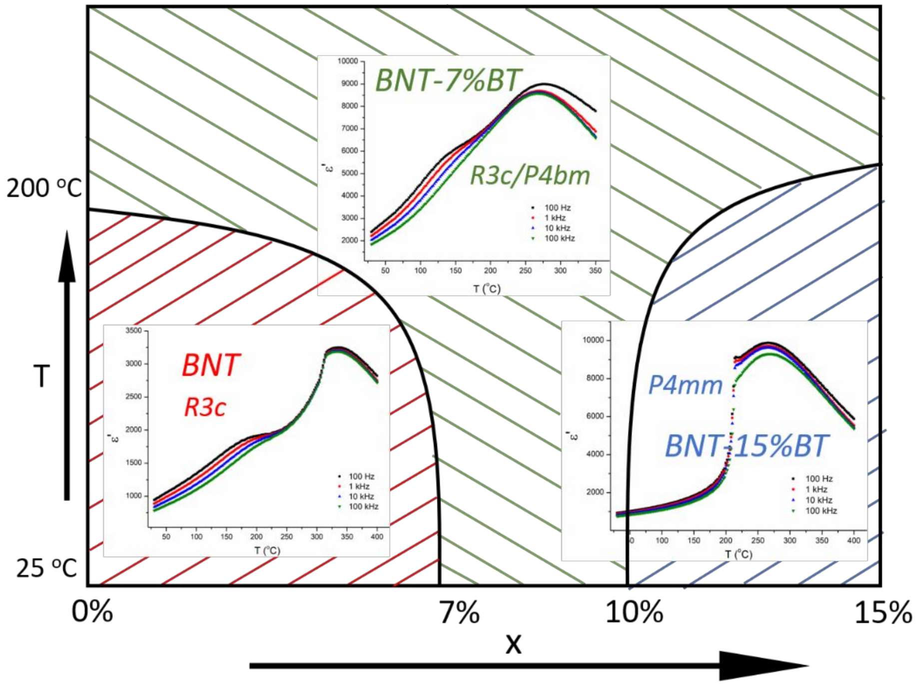

Fig. 1 Phase diagram of BNT-xBT. The dielectric constant measured in the unpoled state of the three studied compositions, pure BNT, BNT-7%BT and BNT-15%BT, are shown as insets.

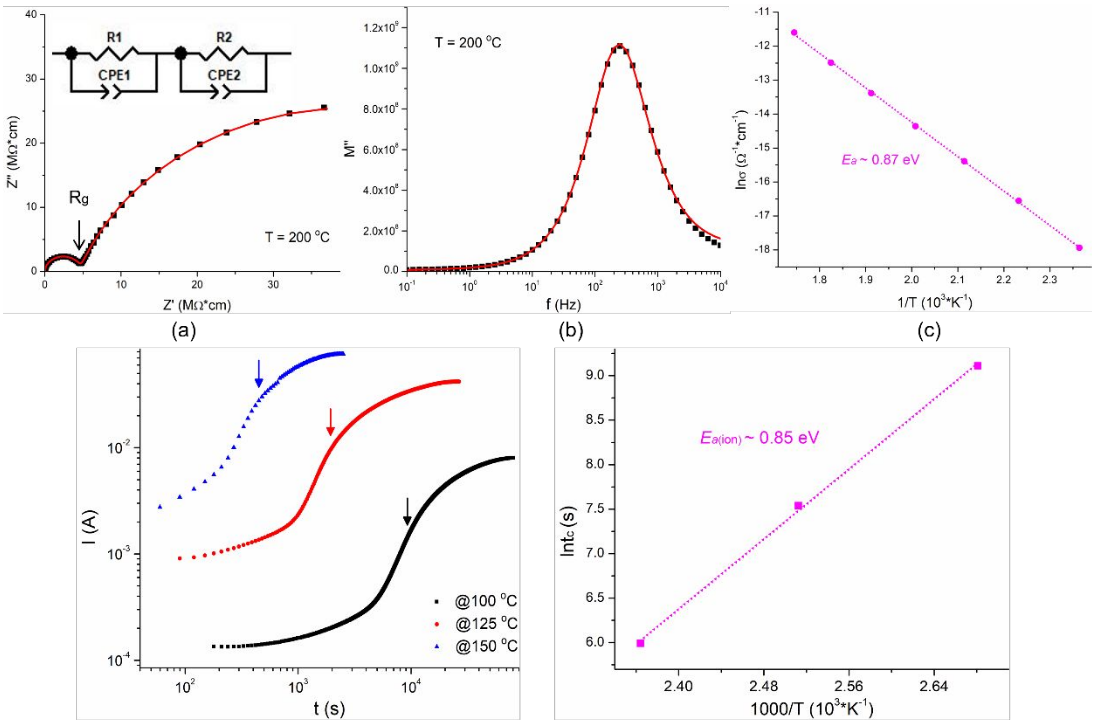

(a) (b) (c)

(d) (e)

Fig. 2 Electrical measurements in pure BNT. (a) fit the Z* plot using the equivalent circuit in the inset; (b) replot the fitting result in M''(f); (c) Arrhenius fitting of the grain conductivity; (d) HALT at different temperatures, with the MTTFs marked by small arrows; (e) Arrhenius fitting of the MTTFs (denoted as t_c).

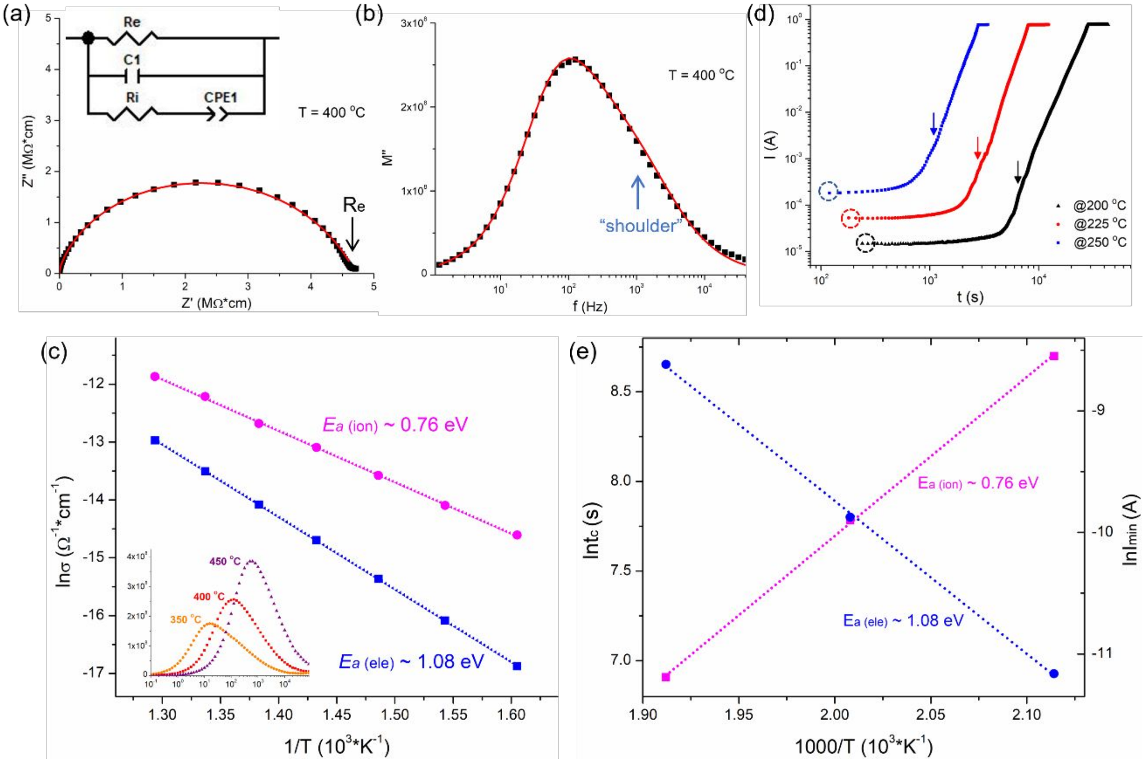

Fig. 3 Electrical measurements in BNT-7%BT. (a) fit the Z* plot using the equivalent circuit in the inset; (b) replot the fitting result in M''(f); (c) Arrhenius fitting of the ionic and electronic conductivity, inset is the modulus at three different temperatures; (d) HALT at different temperatures, with the MTTFs marked by small arrows and the initial leakage currents marked by small circles; (e) Arrhenius fitting of the MTTFs and the initial leakage currents.

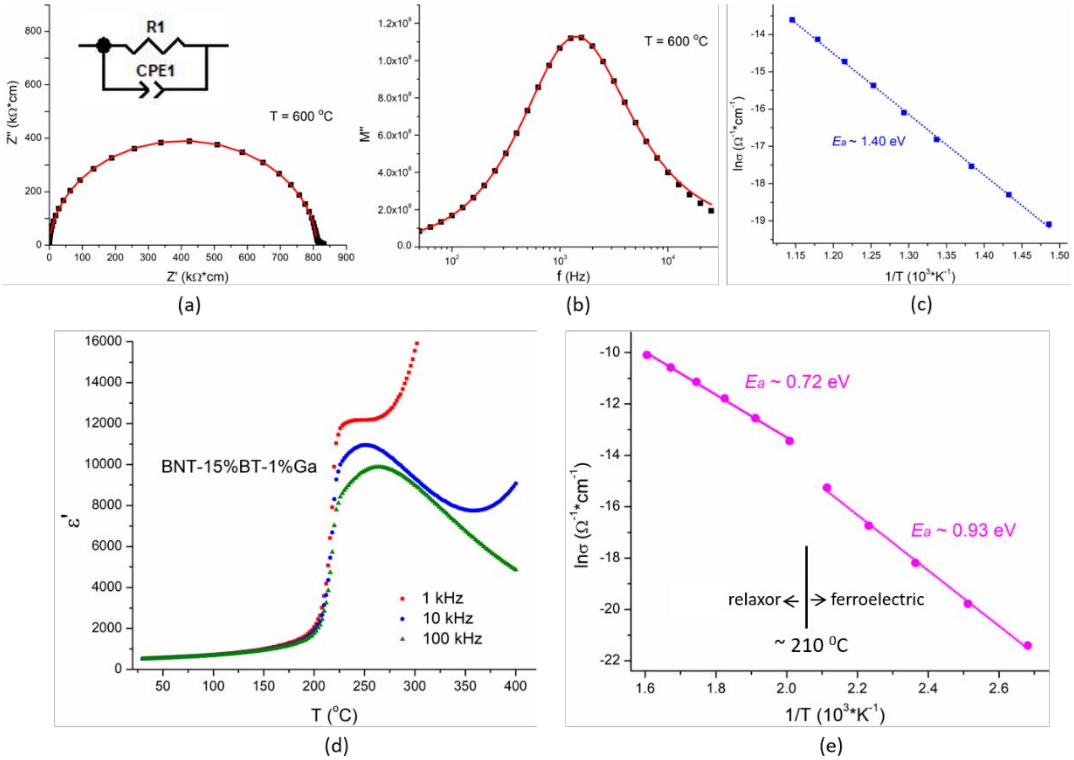

Fig. 4 Electrical measurements in BNT-15%BT. (a) fit the Z* plot using the equivalent circuit in the inset; (b) replot the fitting result in M″(f); (c) Arrhenius fitting of the conductivity of BNT-15%BT; (d) temperature dependent dielectric constant in BNT-15%BT-1%Ga; (e) Arrhenius fitting of the bulk conductivity of BNT-15%BT-1%Ga.

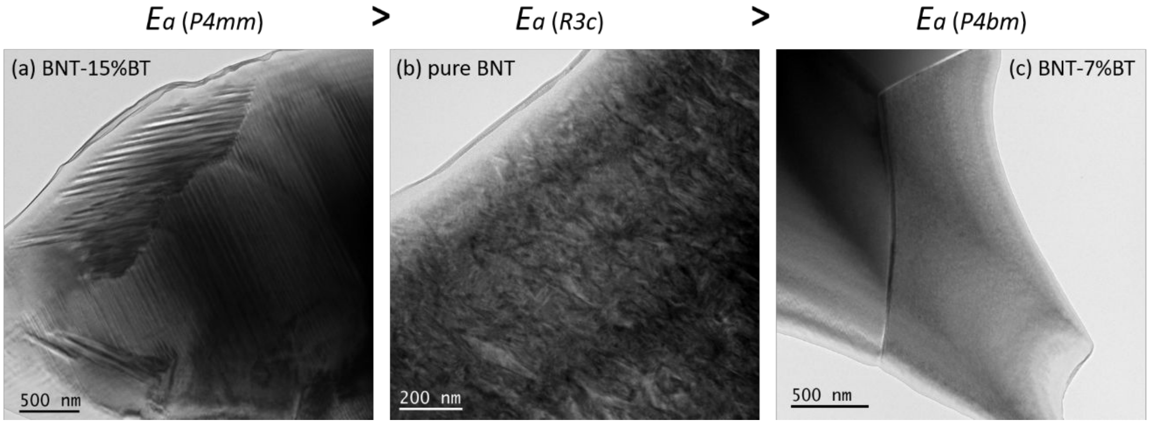

Fig. 5 The domain morphology in (a) BNT-15%BT; (b) pure BNT; (c) BNT-7%BT. E_a is the activation energy for oxygen vacancy migration in each composition.